Granulometry Using Image Transformation Techniques

Andrzej Zadorożny, Hong Zhang, and Martin Jägersand
Department of Computing Science
University of Alberta
Edmonton, Alberta, Canada, T6G 2E8

Abstract

In this paper, we present our preliminary study on using transformation-based techniques for performing granulometry analysis. We examine specifically the problem of the particle size analysis in oil sand images. In contrast to conventional methods of size analysis, we avoid the difficult step of image segmentation and derive information about the size distribution of the particles in the images directly by the transformation techniques of Fourier analysis and scale-space decomposition. We have tested our techniques on both simulated artificial data and real video images, and demonstrated the feasibility of the proposed approaches.

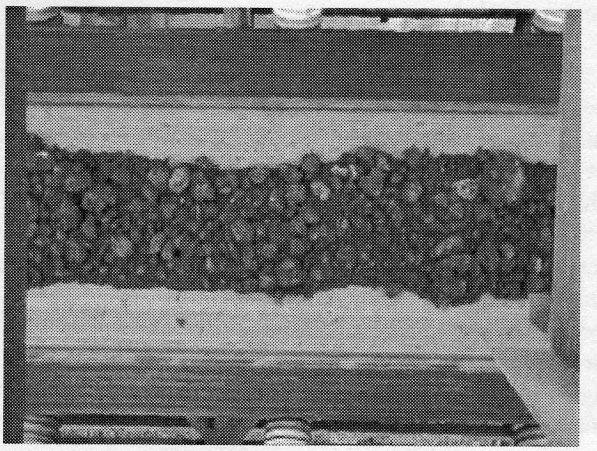

Figure 1: *Oilsand material on a conveyor belt.*

1 Introduction

In this paper, we present two techniques for performing image granulometry, the problem of determining the particle sizes in an image. We specifically focus on the analysis of video streams of oil sands on a conveyor belt (Figure 1), and the computation of statistical size distributions of the oil sand lumps. This work has a direct application in oil sand mining, by providing knowledge to field operators and allowing them to evaluate and optimize oil sand handling equipments.

Although traditional size analysis techniques exist, such as mechanical sieving, centrifugation, and sedimentation, it is highly desirable to use a system based on computer vision to obtain oil sand size information as it does not interfere with or disrupt the production, and allows analysis of a large number of samples, thanks to the relatively high speed of image processing. In addition, a vision-based technique is not invasive, preserving the shape properties of oil sand lumps to be analyzed. Toward this end, a major collaborative research initiative has been in place between the University of Alberta and Syncrude Research (Canada), the world's largest oil producer from oil sand, and a key player in a major industry in the province of Alberta.

There is no known literature on oil sand granulometry using computer vision, except for systems developed for the hard rock industry for analyzing fragmented rocks after blasting [6]. Hard rocks, fortunately, have well-defined edges and their images can be segmented easily using edge-based techniques. In the case of oil sand images, however, edge-based methods fail due to the rich texture of oil sand lumps, and lack of edge information. In addition, since oil sand mining is a 24-hour, outdoor operation, varying lighting and weather conditions play a significant role in the appearance of oil sand. A size analysis system for oil sand based on segmentation must resolve a number of technical challenges that are known to be difficult to computer vision.

In our previous research, we developed a technique for oil sand analysis based on mathematical morphology [2]. We observed that large oil sand lumps appear to be brighter than the fines (small particles) that surround a large lump. This observation led to a morphological segmentation algorithm to delineate individual objects in an oil sand image. There are however several problems with morphological segmentation, as shown in Figure 2. Frequently, for example, small and dark objects cannot be properly segmented, and the areas of the segmented objects are often underestimated. The latter is caused by classifying darker pixels on the perimeter of a lump as not being part of the lump. Other problems include false detection of two objects within one, and classification of a collection of more than one object as

one entity (Figure 2).

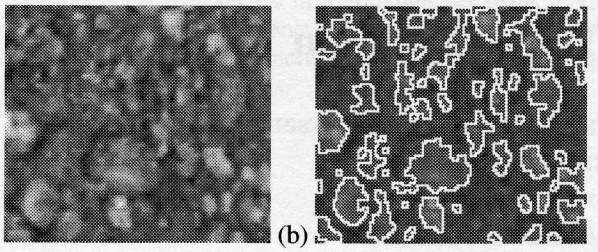

Figure 2: *(a) An oil sand image; (b) Morphological segmentation of (a).*

In this paper, we present our studies on using non-segmentation techniques for granulometry analysis. We examine two transformation-based approaches, namely, Fourier analysis and scale-space decomposition, as alternatives that compute size distribution directly without the difficult step of image segmentation. The rest of the paper is organized as follows. In the next section, we define the two transformation-based approaches and explain how they can be applied to oil sand granulometry. In Section 3, we will present experimental results on both simulated and real images, and in the last section, we will make concluding remarks and outline future work.

2 Transformation-Based Granulometry Analysis

The first technique we have examined is Fourier analysis, which decomposes a signal into its frequency components. In the context of granulometry, generally the presence of large objects yield stronger responses in low frequencies, and weaker responses in high frequencies. Images dominated with small objects should produce opposite result. The second technique we have investigated is scale-space decomposition, which separates an image into information contents at different scales. As the scale is shifted from one to another, objects of different sizes emerge and disappear visually, and this phenomenon can be captured using the Kullback contrast operator.

Since artificial data is both easier to analyze (due to its regularity and low noise content), and can be built to observe a given size distribution, we use artificial data in addition to real data in the experiments. Artificial data comes in the form of intensity and depth profile images. The former simulates data obtained with a vision system, while the latter a laser range finder. As in the case of morphological segmentation [2], local histogram equalization is also applied to real images. This is to minimize the effect of object intensity on the analysis results. The two transformation methods will be tested using both real and artificial data.

2.1 Fourier Power Spectrum Analysis

The 2-D Fourier transform is given by [3]:

$$F(u,v) = \int\int_{-\infty}^{\infty} f(x,y) \exp\left[-2\pi(ux+vy)\sqrt{-1}\right] dxdy$$

and it yields a complex function of the form:

$$F(u,v) = R(u,v) + I(u,v)\sqrt{-1}$$

Using the real and imaginary components, the Fourier power spectrum is computed as follows:

$$P(u,v) = R^2(u,v) + I^2(u,v)$$

Next, the 2-D power spectrum is converted into a 1-D spectrum by performing radial sum on the 2-D spectrum data, for descrete values of r:

$$S(r) = \sum_v \sum_u \begin{cases} P(u,v) & \text{if } r = \lfloor \sqrt{(u_0-u)^2+(v_0-v)^2} \rfloor \\ 0 & \text{otherwise} \end{cases}$$

where (u_o, v_o) represents the location of the center of the 2-D spectrum. An example output of such computation is shown in Figure 4, when the Fourier analysis is applied to the image in Figure 3.

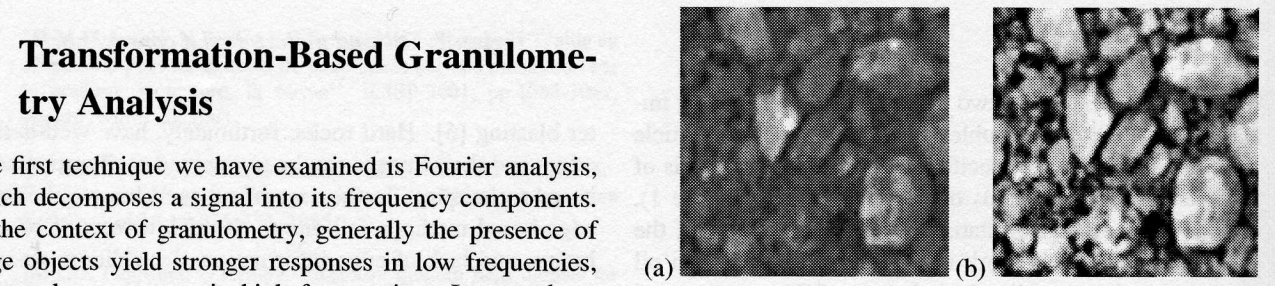

Figure 3: *(a) An oil sand image; (b) local histogram equalization of (a).*

For purposes of object size distribution, wavelength distribution is used as opposed to frequency spectrum. The wavelength distribution is obtained in the following way, for descrete values of w:

$$W(w) = \sum_v \sum_u \begin{cases} P(u,v) & \text{if } w = 1 + \lfloor \frac{r_{max}-1}{\sqrt{(u_0-u)^2+(v_0-v)^2}} \rfloor \\ 0 & \text{otherwise} \end{cases}$$

where r_{max} is the maximum radius (i.e. distance between the center (u_0, v_0) and the edge of the 2-D Fourier power spectrum).

Quantization of wavelength distributions into distribution histogram slots introduces an aliasing effect. In order to avoid this effect, cumulative wavelength distributions are used instead. The latter is more convenient in modelling industrial sieving filters, and thus of greater interest in particle

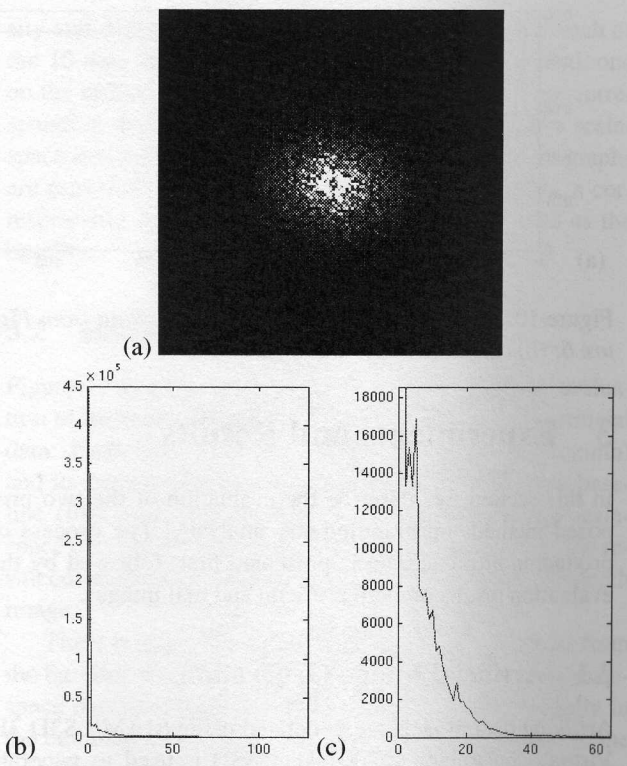

Figure 4: *(a) An enhanced image of Fourier power spectrum of the image from Figure 3 (b); (b) radial sum of the Fourier power spectrum data; (c) a subgraph of (b), showing more relevant features.*

size analysis. The cumulative wavelength distribution is recursively defined as, for discrete values of x:

$$C(1) = W(1), C(x) = C(x-1) + W(x)$$

Figure 5 illustrates wavelength distribution computed from the data in Figure 4.

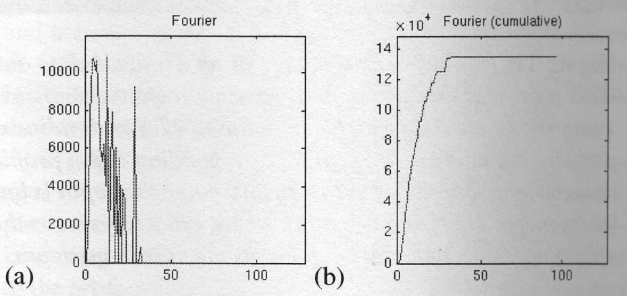

Figure 5: *(a) Wavelength distribution of data in Figure 4; (b) cumulative wavelength distribution of data in Figure 4.*

2.2 Scale-Space Decomposition

The second technique we have used to analyze oil sand data is scale-space decomposition. Figure 6 illustrates an example of scale-space expansion. The scale-space expansion is achieved by reducing the resolution of the original image, not by decreasing image dimensions, but rather by convolving an image with a low-pass filter [4]. A very efficient way to implement the convolution is to perform the operation in 1-D instead of 2-D. First, the 1-D convolution with a Gaussian filter is applied to the columns of the image. Next the same operation is applied to the rows of the resultant image, achieving the desired 2-D effect.

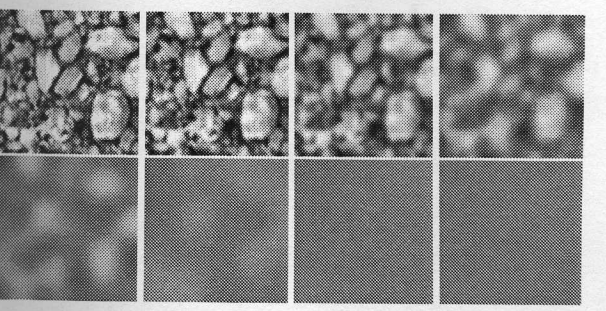

Figure 6: *A locally equalized oil sand image (from Figure 3) represented in scales ranging from 1 to 128.*

The 1-D convolution can be performed very efficiently by a box averaging filter, such as the one shown in Figure 7 [4]. An approximation of a Gaussian filter is obtained via several convolutions of the box with itself. Figure 8 illustrates that as few as two convolutions yield a reasonable approximation. The box filter is normalized, resulting in a Gaussian filter that is normalized as well. Different resolutions of the scale-space expansion are obtained by varying the size of the box filter, which in turn affects the standard deviation of the Gaussian filter.

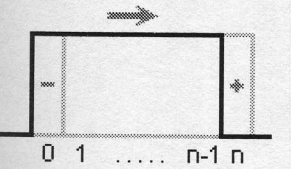

Figure 7: *An example of a box averaging filter of size n sliding right. In this case, the shifting is achieved by removing component 0 (left-most component of the average), and adding component n (the new value immediately to the right of the box).*

Information difference between various scales of the scale-space expansion is measured using the Kullback contrast operator:

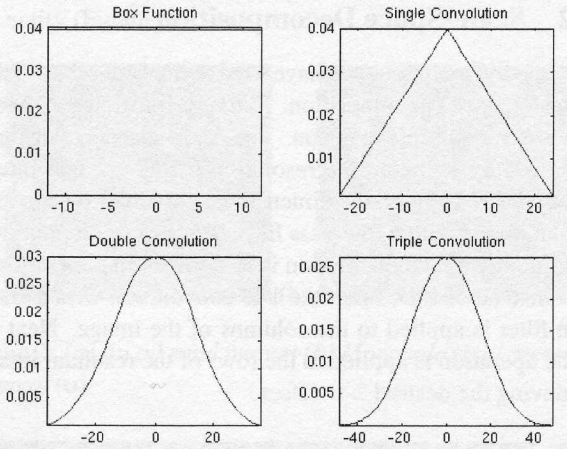

Figure 8: *Successive iterations of 1-D convolution of a box function.*

$$K[Q,P] = \int_x p(x) \log \frac{p(x)}{q(x)} dx$$

Q and P are the intensity input images of consecutive scales to be compared (see Figure 6). Images are compared on a pixel-by-pixel basis, iterating over pixel x. Each such image is treated as a probability distribution, and thus must first be normalized.

Application of this operator to various scales can be seen in Figure 9, for the scale-space expansion in Figure 6. Kullback contrast response (Figure 10) is calculated by summing up all the values of K[Q, P], and it represents the distribution of objects that appear at different sizes.

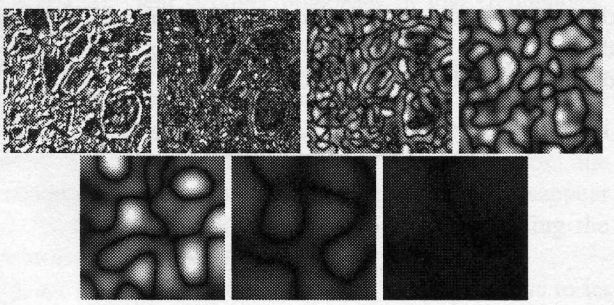

Figure 9: *Kullback contrast response for consecutive pairs of scale-space images from Figure 6.*

The scale-space decomposition used in [4] and [5] forces the cut-off frequency of the low-pass filter to vary as integer powers of 2. Although, such formulation provides only a few sampling points, it simplifies the encapsulation of information change between consecutive scales. We have adopted the same convention in our experiments.

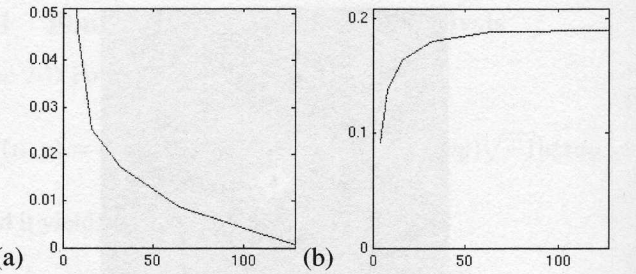

Figure 10: *(a) Kullback contrast response of data from Figure 6; (b) cumulative version of (a).*

3 Experiments and Results

In this section, we describe the evaluation of the two proposed methods on granulometry analysis. The process of producing artificial data is presented first, followed by the evaluation results on both artificial and real images.

3.1 Artificial Image Generation

Artificial data models are generated using SIAMS S3D 3D Virtual Constructor ©2001 [1]. S3D is used to generate data using Gaussian distribution of sphere radii given a desired mean radius and standard deviation (STD). The software makes sure that no spheres overlap each other and that the whole structure is statically balanced. The data model can then be used to generate intensity or depth profile images (such as the ones shown in Figure 11), to serve as a ground truth for evaluation purposes.

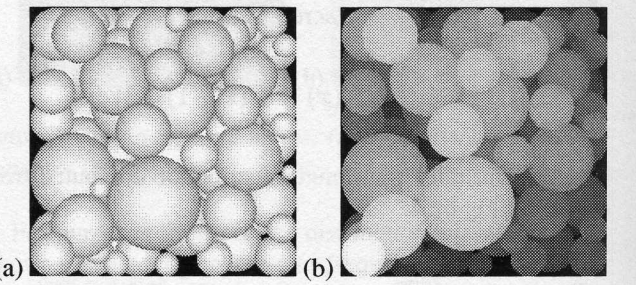

Figure 11: *(a) An intensity image of an artificial data set. This particular model is generated using a Gaussian distribution of sphere radii with mean radius of 22.5 and radius standard deviation of 10.5. (b) A corresponding depth profile image of the data shown in (a). In this image the depth is linearly mapped to pixel intensities, where white represents the minimum depth, and black represents the maximum depth.*

Ten artificial data models were generated in our experiments. In the first five, the mean radius is varied, while the STD is kept constant. In the last five, the mean radius is kept constant, but STD is varied. Figure 11 shows the inten-

sity and depth images for artificial data set 10. For each of the 10 data models, two experiments were performed, one on the artificial intensity image, and the other on the corresponding depth image. For each experiment, both a scale-space decomposition and a Fourier power spectrum graphs are provided. In addition, for comparison purposes, a corresponding graph of actual distribution is provided as the baseline.

3.2 Results on Artificial Images

Figure 12 and Figure 13 show typical results of the evaluation of the two transformation-based techniques on artificial data. Each figure shows the size distribution (left column) and its cumulative integration (right column), for the baseline (first row), Fourier analysis (middle row), and scale-space decomposition (bottom row). Figure 12 shows the result corresponding to intensity image, and Figure 13 to depth image.

There is generally good agreement between results from the baseline and the Fourier analysis. The result from scale-space decomposition follows a similar trend, especially in the cumulative distribution, although it is less similar to the baseline than Fourier analysis. This is due in part to the coarse nature of scale-space analysis, which forces the classification of particles into seven sizes only that are integer powers of 2 between 0 and 128. Another reason for this difference is that the artificial data contain no fines, whereas the Fourier analysis and scale-space decomposition are designed to assume the presence of fines. In general, it is obvious that the both proposed approaches are feasible for granulometry analysis.

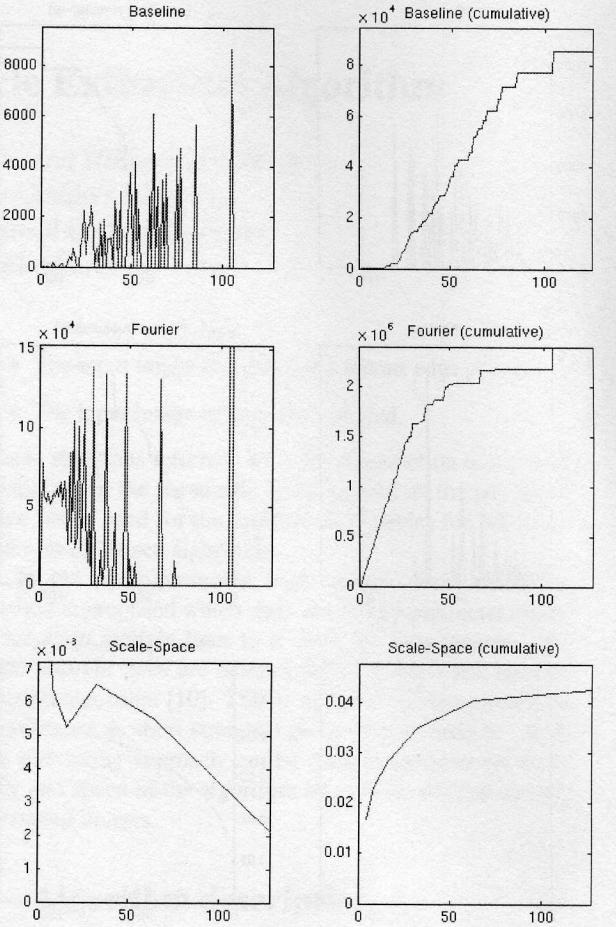

Figure 12: *Experimental results corresponding to the intensity data of Figure 11(a).*

3.3 Real Data

For real data, seven images of oil sands were chosen, with a varying distribution of object sizes. For each image, two experiments were performed, one on the original input image, and one on a histogram-equalized version of the input image. For each experiment, both a scale-space decomposition and a Fourier power spectrum graphs are provided. Since no information about the actual distribution of object sizes is available, the result of morphological segmentation [2] is used for comparison purposes as the baseline.

Figure 3 shows the original and histogram equalized images for real data set 3, which is described here as an example, and the experimental results corresponding to the equalized image (Figure 3(b)) are graphed in Figure 14. Similar to the artificial data case, the left column of Figure 14 shows the size distributions, and the right column shows the corresponding cumulative integrations. The three pairs of figures represent the baseline from morphology analysis, Fourier analysis, and scale-space decomposition, respectively. Note that the smoothness of the size distribution in scale-space decomposition is once again mostly due to the scales being necessarily integer powers of 2. In all cases, the results are also quite satisfactory, with respect to the chosen baseline.

4 Conclusions and Future Work

We have presented in this paper our preliminary study of two transformation based techniques for granulometry analysis of oil sand materials. The main advantage of the techniques is that they avoid the difficult step of image segmentation in deriving a particle size distribution of an image. The results are only qualitative, since they do not yield direct information about object sizes. Experiments based on both simulated data and real data have established the general feasibility of the two proposed approaches.

Future work will include further refinement of the two transformation-based algorithms, to model more accurately fine particles, which were found to be difficult to handle.

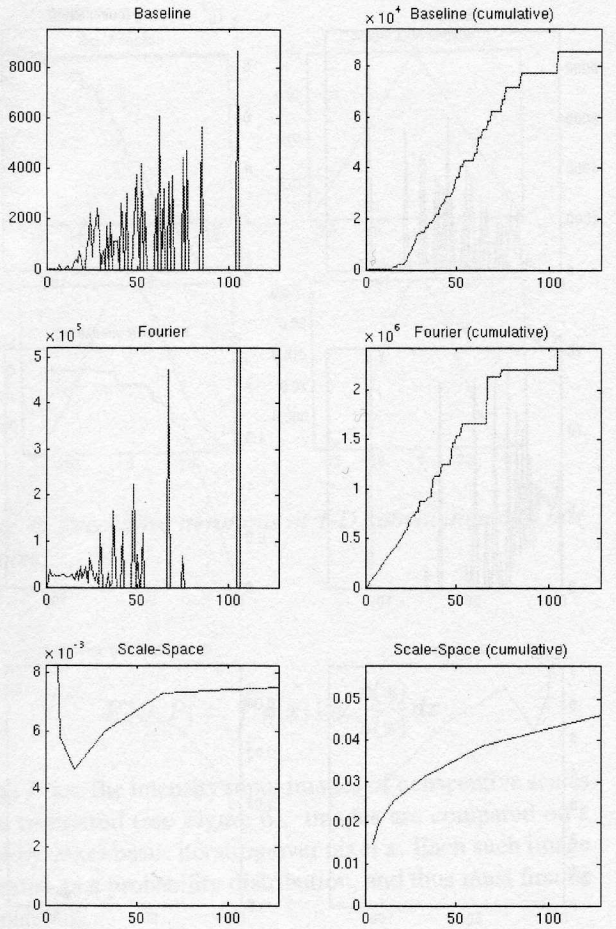

Figure 13: *Experimental results corresponding to the depth data of Figure 11(b).*

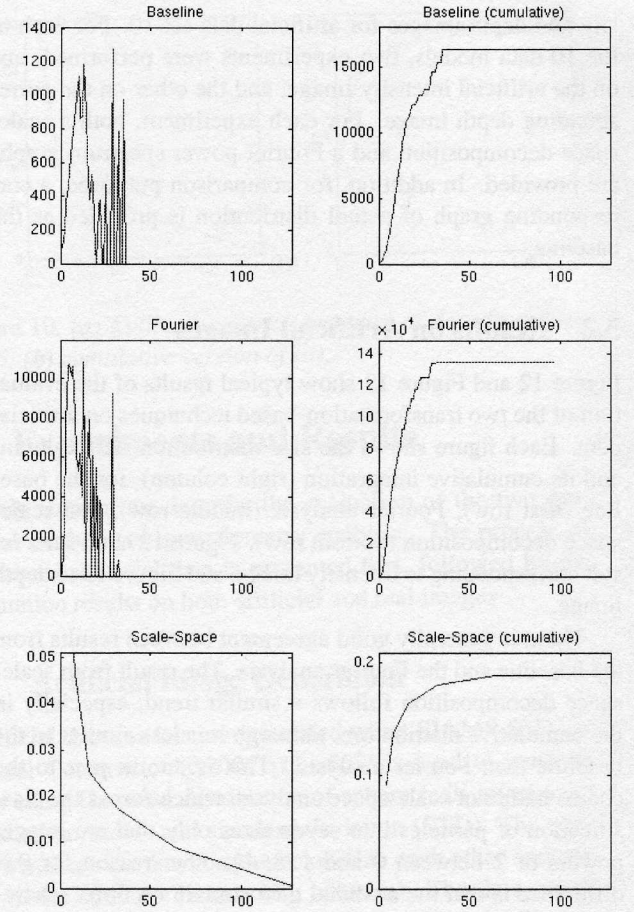

Figure 14: *Experimental results corresponding to the equalized image Figure 3(b).*

We will also explore alternative formulations of scale-space decomposition to produce a size distribution of higher resolution. Additionally, we will investigate derivation of quantitative information about object sizes from transformation based techniques. As well, we will attempt to establish accurate baselines for real images in order to evaluate granulometry algorithms objectively. Finally, we will examine other transformation techniques such as wavelet transform for their feasibility in granulometry analysis.

References

[1] D.M. Alievsky, I.G. Kamenin, R.M. Kadushnikov, V.M. Alievsky, "Geometrical Modelling of Spheropolyhedra Close Packing", *International Workshop on modelling of metal powder forming processes*, 1997.

[2] F. Dornaika, and H. Zhang, "Granulometry using Mathematical Morphology and Motion", in *Proc. 2000 IAPR Workshop on Machine Vision Applications*, Tokyo, Japan, November 28-30, 2000, pp. 51–54.

[3] R.C. Gonzalez, and R.E. Woods, *Digital Image Processing*, Addison-Wesley, 1992.

[4] M. Jägersand, "A Scale Decomposed Information Measure in Images", *Proc. ARPA Image Understanding Workshop*, 1994.

[5] M. Jägersand, "Saliency Maps and Attention Selection in Scale and Spatial Coordinates: An Information Theoretic Approach", *ICCV*, 1995.

[6] N.H. Maerz, T.C. Palangio, J.A. Franklin, "WipFrag image based granulometry system", *Measurement of Blast Fragmentation*, pp. 91–99, Franklin & Katsabanis (eds), 1996.